

Ab initio study of structural, electronic, thermo-elastic and optical properties of Pt₃Zr intermetallic compound

Wahiba Metiri^{1,†} and Khaled Cheikh^{2,‡}

¹Département de Physique, Faculté des Sciences, Université 20 août 1955-Skikda BP 26, Route El-Hadaiek, 21000 Skikda, Algeria

²Département de Technologie, Faculté de Technologie, Université 20 août 1955-Skikda BP 26, Route El-Hadaiek, 21000 Skikda, Algeria

(Received 11 November 2019; revised manuscript received 28 January 2020; accepted manuscript online 3 February 2020)

Structural, elastic, electronic and optical properties of the Pt₃Zr intermetallic compound are investigated using first principles calculations based on the density functional theory (DFT) within the generalized gradient approximation (GGA) and the local density approximation (LDA). The Pt₃Zr compound is predicted to be of cubic L1₂ and hexagonal D0₂₄ structures. The calculated equilibrium ground-state properties (lattice parameters a and c , bulk modulus B and its pressure derivative B' , formation enthalpy ΔH) of the Pt₃Zr compound, for both cubic and hexagonal phases, show good agreement with the experimental results and other theoretical data. Elastic constants (C_{11} , C_{12} , C_{13} , C_{33} , C_{44} , and C_{55}) are calculated. The predicted elastic properties such as Young's modulus E and shear modulus G_H , Poisson ratio ν , anisotropic ratio A , Kleinman parameter ξ , Cauchy pressure ($C_{12} - C_{44}$), ratios B/C_{44} and B/G , and Vickers hardness H_v indicate the stiffness, hardness and ductility of the compound. Thermal characteristic parameters such as Debye temperature θ_D and melting temperature T_m are computed. Electronic properties such as density of states (DOS) and electronic specific heat γ are also reported. The calculated results reveal that the Fermi level is on the pseudogap for the D0₂₄ structure and on the antibonding side for the L1₂ structure. The optical property functions (real part $\epsilon_1(\omega)$ and imaginary part $\epsilon_2(\omega)$ of dielectric function), optical conductivity $\sigma(\omega)$, refraction index $n(\omega)$, reflectivity $R(\omega)$, absorption $\alpha(\omega)$ and extinction coefficients $k(\omega)$ and loss function $L(\omega)$ are also investigated for the first time for Pt₃Zr in a large gamme of energy from 0 to 70 eV.

Keywords: density functional theory, intermetallic, density of states, L1₂, D0₂₄, optical properties

PACS: 71.15.Mb, 71.20.LP, 71.20.-b

DOI: 10.1088/1674-1056/ab7223

1. Introduction

Platinum group metals (PGMs) and platinum-based alloys, as high temperature structural materials, have attracted considerable attention in industrial applications^[1-6] (automotive, aeronautic, aerospace, catalysis etc.). They exhibit exceptional physical, chemical and mechanical properties such as high melting point, high density, high strength, low reactivity and good oxidation and corrosion resistance.^[5-16] Melting point of Pt is about 1760 °C, which is higher than that of pure nickel (1450 °C), and a young modulus is about 164 GPa.^[17-20] Alloyed Pt (early transition metal) with an element from groups 4B and 5B such as Ti, V, Zr, Nb, Hf, and Ta (late transition metals) could form very stable alloys (Engel-Brewer alloys).^[21,22] Pt-Zr alloys, especially Pt₃Zr, show enhanced thermal and mechanical properties compared with Ni-based alloys. The Pt₃Zr melting temperature in the L1₂ cubic structure is up to 2600 °C and the Young modulus is about 260 GPa, which are much higher than those of other Pt-based compounds.^[23,24]

Many experimental and theoretical works have been effected to investigate basic properties of Pt₃Zr in the L1₂ and D0₂₄ structures. Bai *et al.* have studied the structural properties, formation enthalpies, elastic constants and bulk modulus of Pt-Zr alloys in stable and hypothetical phases using the CASTEP code.^[25] First principles calculations have been im-

plemented with the CASTEP code by Pan *et al.* to study a new structure and oxidation mechanism of the Pt₃Zr compound.^[26] Interfacial stability, electronic structure and bond characteristics of Pt₃Zr (111)/Pt (111) interfaces have been investigated by Pan *et al.* using ab-initio calculations.^[27] Using high resolution x-ray photoelectron spectroscopy, temperature programmed desorption, scanning tunneling microscopy and density functional theory, Li *et al.* studied growth of an ultrathin zirconia film on Pt₃Zr.^[28] Antlinger *et al.* investigated the surface of pure and oxidized Pt₃Zr (0001) by scanning tunneling microscopy (STM).^[29] However, there are insufficient experimental and computational data for realizing Pt₃Zr electronic and elastic properties. Moreover, neither experimental nor theoretical results on their optical properties are available in the literature.

In this article, we investigate structural, elastic, thermal, electronic and optical properties of the Pt₃Zr intermetallic compound in cubic and hexagonal structures. Our work is based on the first principles calculations considered as the most powerful method for research of materials properties.^[30,31]

2. Computational details

In the present paper, computations of structural, elastic, electronic and optical properties of the Pt₃Zr intermetallic

[†]Corresponding author. E-mail: wahiba.metiri@yahoo.fr

[‡]Corresponding author. E-mail: cheikh.khaled@yahoo.fr

compound were carried out using first principle calculations. All calculations are based on density functional theory (DFT) employing the full potential linearized augmented plane wave (FP-LAPW) method implemented in the WIEN2k code.^[32,33] Exchange correlation functional was treated within the generalized gradient approximation (GGA) with the Perdew–Burke–Ermerhof (PBE) and the local density approximation (LDA).^[34,35] The Pt_3Zr compound is found to be crystalline in the $L1_2$ cubic structure (space group of $Pm\bar{3}m$) with lattice parameter $a = 4.051 \text{ \AA}$ ^[36] and in the $D0_{24}$ hexagonal structure (space group of $P6_3/mmc$) with lattice parameters $a = 5.653 \text{ \AA}$ and $b = 9.347 \text{ \AA}$.^[5] Muffin–Tin (MT) spheres radii R_{MT} were taken as 2.5 a.u. for Pt and Zr atoms. Total energies are converged at 10^{-4} Ry. Integrations in the Brillouin zone were performed using special k -point generated with $12 \times 12 \times 12$ and $10 \times 10 \times 5$ mesh grids for cubic and hexagonal structures, respectively. The plane wave expansion parameter $R_{\text{MT}} \times K_{\text{max}}$, which controls the size of the basis sets in our calculations, was taken to be 7. The wave function inside the MT spheres was chosen up to $l_{\text{max}} = 10$. The charge density was expanded up to $G_{\text{max}} = 12$. The valence electron configurations were $[\text{Zr}] = 4d^2 5s^2$ and $[\text{Pt}] = 5d^9 6s^1$.

3. Results and discussion

3.1. Structural properties

Crystal structures of Pt_3Zr in Cubic and hexagonal phases are shown in Fig. 1. For the $L1_2$ structure, Pt and Zr occupying the Wyckoff site of $3c$ $(0, 1/2, 1/2)$ and $1a$ $(0, 0, 0)$, respectively. For the $D0_{24}$ structure, the atomic positions are $6g$ $(1/2, 0, 0)$, $6h$ $(0.83, 2/3, 1/4)$ and $2a$ $(0, 0, 0)$, $2c$ $(1/3, 2/3, 1/4)$ for Pt and Zr, respectively. The equilibrium lattice constants of the Pt_3Zr compound have been computed by optimizing volume through Murnaghan’s equation of state. The calculated total energies versus volume for cubic and hexagonal Pt_3Zr using (a) PBE-GGA and (b) LDA approximations are plotted in Fig. 2. We show that the $D0_{24}$ phase of the Pt_3Zr compound is slightly lower in energy than the $L1_2$ phase. The optimized ground state properties such as lattice parameters a and c , bulk modulus B and its pressure derivative B' , formation enthalpy ΔH_f compared with the experimental and theoretical data are listed in Table 1. We find that there is an excellent agreement between our results and the available data. It can be seen that the calculated equilibrium lattice parameter a of the Pt_3Zr $L1_2$ structure using GGA (LDA) deviates from the experimental value by $+0.12\%$ (-2.02%). However, the calculated equilibrium lattice parameters a and c of $D0_{24}$ - Pt_3Zr deviate from the experimental value by $+1.23\%$ (-0.61%) and -0.18% (-1.57%), respectively, using the GGA (LDA) method. We have not found experimental values of B' to confirm our results.

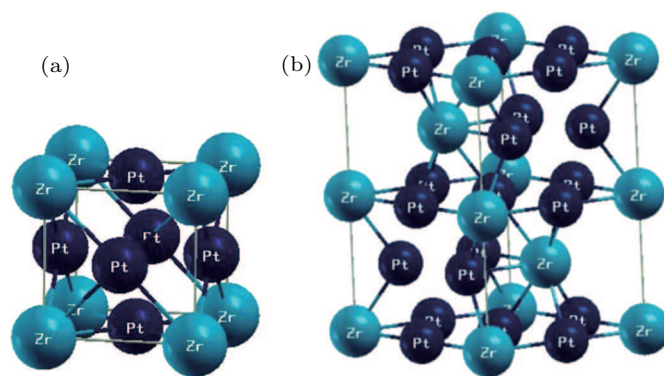


Fig. 1. Crystal structures of Pt_3Zr : (a) cubic $L1_2$ and (b) hexagonal $D0_{24}$.

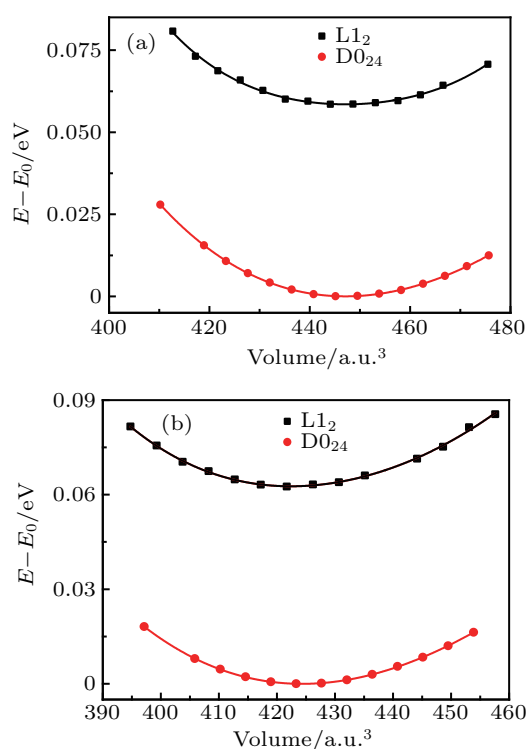


Fig. 2. Total energy versus volume per unit cell of $L1_2$ - Pt_3Zr and $D0_{24}$ - Pt_3Zr using (a) PBE-GGA and (b) LDA.

From the ground-state total energy, the formation enthalpy of Pt_3Zr is given as follows:^[37]

$$\Delta H_f^\phi(\text{Pt}_3\text{Zr}) = \frac{1}{4}E_{\text{Pt}_3\text{Zr}}^\phi - \left[\frac{3}{4}E_{\text{Pt}}^\phi + \frac{1}{4}E_{\text{Zr}}^\phi \right], \quad (1)$$

where $E_{\text{Pt}_3\text{Zr}}^\phi$ is the total energy of the Pt_3Zr compound with ϕ structure, E_{Pt}^ϕ and E_{Zr}^ϕ are total energies per atom of Pt and Zr with ϕ and ϕ structures, respectively. The calculated values of ΔH_f for the cubic structure are in good agreement with other theoretical data. However, our result for hexagonal structure is relatively smaller than those reported in Ref. [25]. We find that the ΔH_f of the Pt_3Zr compound in the $D0_{24}$ phase is lower than that in the $L1_2$ phase, which indicates that Pt_3Zr in the hexagonal structure is more stable than that in the cubic structure.

Table 1. Calculated equilibrium elastic constants (a , c), bulk modulus B and its derivative B' , and formation enthalpy ΔH_f for cubic and hexagonal Pt₃Zr.

Compound		Crystalline parameters		B/GPa	B'	$\Delta H_f/(\text{eV}/\text{atm})$
		$a/\text{\AA}$	$c/\text{\AA}$			
Pt ₃ Zr in L1 ₂	present GGA	4.046		219.07	4.66	-1.105
	present LDA	3.969		262.25	5.46	-1.140
	experimental ^[36]	4.051				
	other ^[5,24-27,38,39]	4.055 ^a , 4.061 ^a , 3.980 ^b		232 ^a , 230 ^a		-1.100 ^a , -0.98 ^a , -1.03 ^a
Pt ₃ Zr in D0 ₂₄	present GGA	5.723	9.330	226.39	4.54	-1.322
	present LDA	5.618	9.200	265.00	5.00	-1.356
	experimental ^[5]	5.653	9.347 ^[5]			
	other ^[25,26,29]	5.729 ^a , 5.742 ^a	9.364 ^a , 9.398 ^a	226 ^a		-1.108 ^a

^aData from the PBE-GGA method. ^bData from the LDA method.

3.2. Elastic properties

Elastic constants can be used to measure material's resistance and mechanical stability under compression. Moreover, elastic constants of materials can offer important information about their mechanical and dynamical behavior. For cubic systems, there are three independent elastic constants C_{ij} , namely C_{11} , C_{12} and C_{44} . However, there are five independent elastic constants C_{ij} for hexagonal structures, namely C_{11} , C_{12} , C_{13} , C_{33} , and C_{55} . Necessary mechanical stability criteria for cubic and hexagonal crystal systems are $C_{11} - C_{12} > 0$, $C_{11} + 2C_{12} > 0$, $C_{44} > 0$ and $C_{11} > |C_{12}|$, $2C_{13}^2 < C_{33}(C_{11} + C_{12})$, $C_{55} > 0$, respectively.^[40,41] The IRelast package contributed by Jamal *et al.*^[42] has been used to calculate the equilibrium elastic constants of Pt₃Zr using the GGA and LDA approximations. We use a dense mesh of 165 and 84 k -points in the irreducible Brillouin zone for cubic and hexagonal structures, respectively. The equilibrium calculated values of C_{ij} for cubic and hexagonal Pt₃Zr using the GGA and LDA methods are given in Table 2. It is clear that our results coincide very well with the experimental and theoretical data. Moreover, our results satisfy the mechanical stability conditions indicating the stability of the studied compound in cubic and hexagonal structures. It is known that C_{11} and C_{33} reflect the unidirectional compression resistance along the principle crystallographic direction while C_{44} (C_{55} for hexagonal phase) describes the crystal resistance to the shear strain. It is found that C_{11} in the cubic (hexagonal) system is 2.5 (5) times higher than C_{44} (C_{55}), signifying that this compound presents a stronger resistance to the unidirectional compression compared to the pure shear deformation.

Elastic properties were investigated using the Voigt-Reuss-Hill (VRH) approximation.^[43] Hill's shear G_H and bulk moduli B_H can be expressed as the average between the Voigt^[44] and Reuss^[45] bounds as follows: $G_H = \frac{1}{2}(G_V + G_R)$, $B_H = \frac{1}{2}(B_V + B_R)$. For cubic phases, G_V , B_V , G_R and B_R can be written as

$$B_V = B_R = \frac{1}{3}(C_{11} + 2C_{12}), \quad (2)$$

$$G_V = \frac{1}{5}(C_{11} - C_{12} + 3C_{44}), \quad (3)$$

$$G_R = \frac{5(C_{11} - C_{12})C_{44}}{4C_{44} + 3(C_{11} - C_{12})}. \quad (4)$$

For the hexagonal system, the corresponding formulas are as follows:

$$G_V = \frac{1}{30}[M + 12C_{55} + 6(C_{11} - C_{12})], \quad (5)$$

$$B_V = \frac{1}{9}[2(C_{11} + C_{12}) + 4C_{13} + C_{33}], \quad (6)$$

$$G_R = \frac{\frac{5}{4}[C^2 C_{55}(C_{11} - C_{12})]}{[\frac{3}{2}B_V C_{55}(C_{11} - C_{12}) + C^2 [C_{55} + \frac{1}{2}(C_{11} - C_{12})]}], \quad (7)$$

$$B_R = \frac{C^2}{M}, \quad (8)$$

where $C^2 = (C_{11} + C_{12})C_{33} - 2C_{13}^2$ and $M = C_{11} + 2C_{33} - 4C_{13}$.

Table 2. Calculated elastic constants of Pt₃Zr (in units of GPa).

Structure		C_{11}	C_{12}	C_{13}	C_{33}	C_{44}	C_{55}
L1 ₂	present GGA	357.38	181.96			139.86	
	present LDA	401.52	206.17			156.65	
	other ^[25]	340 ^a	175 ^a			98 ^a , 119 ^a	
D0 ₂₄	present GGA	357.19	177.97	154.85	399.22		70.32
	present LDA	416.31	219.57	151.05	448.75		77.21
	other ^[25]	337 ^a	159 ^a	147 ^a	375 ^a		88 ^a

^a Data from the PBE-GGA method. ^bData from the LDA method.

The calculated bulk modulus B_H and shear modulus G_H of cubic and hexagonal Pt₃Zr are listed in Table 2. The bulk moduli represent the material resistance to the volume change under pressure, however the shear moduli are measure of resistance to shape change under shear stress. Moreover, these parameters can measure the crystal hardness. Therefore, our results indicate that the Pt₃Zr has higher hardness in the cubic structure than that in the hexagonal one. The shear modulus values imply that Pt₃Zr has excellent shear deformation resistance.

Other significant elastic parameters such as Young's modulus E , Poisson's ratio ν , Pugh's index G/B , machinability index B/C_{44} , Cauchy pressure $C_{12} - C_{44}$ ($C_{12} - C_{55}$ for the hexagonal structure), anisotropic ratio A , Kleinman parameter ξ , and Vickers hardness H_V are investigated for the cubic and hexagonal structures using the GGA and LDA approximations. The calculated elastic properties together with other experimental and theoretical data are given in Table 3. From Table 3, the LDA calculations are larger than those of GGA. We can conclude that the smaller the lattice parameter, the higher

the elastic properties. Young's modulus and Poisson's ratio ν are calculated using the following relations:^[46,47]

$$E = \frac{9B_H G_H}{3B_H + G_H}, \quad (9)$$

$$\nu = \frac{3B - 2G}{6B + 2G}. \quad (10)$$

Young's modulus E , namely elasticity modulus, is defined as the ratio of the tensile stress to the corresponding tensile strain. It is an important property providing the material stiffness. The calculated Young moduli with the GGA (LDA) method are 300 GPa (335 GPa) for the L1₂ structure and 230 GPa (261 GPa) for the D0₂₄ phase, indicating that Pt₃Zr has a strong stiffness higher than other^[24] Pt–Zr alloys. Moreover, Pt₃Zr in the cubic structure is stiffer than that in the hexagonal structure. Our result for the L1₂ structure coincides well with that obtained by Pan *et al.*^[24,27] Poisson's ratio, Pugh's index and the Cauchy pressure are good indicators for ductile/brittle nature of materials. Poisson's ratio is smaller than 0.26 for brittle materials, otherwise the material behaves in a ductile manner. Furthermore, Poisson's ratio gives information about the characteristics of the bonding in materials. For covalent materials, Poisson's ratio has a small value ($\nu = 0.1$), whereas for ionic compounds, it has a typical value of 0.25. For metallic materials, the ν value is typically 0.33. In our case, the ν values for cubic and hexagonal structures are 0.29 and 0.33, respectively, indicating a considerable metallic contribution to intra-atomic bonding for the Pt₃Zr compound. According to Pugh's index, the material will be brittle (ductile) if the B/G ratio is smaller (higher) than 1.75. Our calculated B/G values are above 1.75 for the cubic and hexagonal structures, indicating a ductile character. The mechanability index^[48] B/C_{44} (C_{55} for the hexagonal structure) may be used as a measure of plasticity and a good indicator of lubricating properties.^[49,50] For the cubic and hexagonal structures, the B/C_{44} values are 1.72 and 3.29, respectively. This means that Pt₃Zr is a good lubricant in the hexagonal structure while it has a low lubricating ratio in the cubic structure (compared to gold which has a wonderful lubricating properties of 4.17).^[51] Moreover, the calculated values of Cauchy pressure are positive, which proves the ductile and metallic behavior of the Pt₃Zr compound.

The Zener anisotropy factor A is an elastic parameter used to measure the degree of elastic anisotropy in solids. A

is highly correlated with the possibility to introduce microcracks in materials. For completely isotropic materials, A takes the value of 1, however for anisotropic materials, A differs from the unity.^[48] For the cubic structure, A reads^[52]

$$A = \frac{2C_{44}}{C_{11} - C_{12}}. \quad (11)$$

However, for the hexagonal structure, there are three anisotropy factors A_1 , A_2 and A_3 corresponding to three shear planes: $\{100\}$, $\{010\}$ and $\{001\}$ between $\langle 011 \rangle$ and $\langle 010 \rangle$, $\langle 101 \rangle$ and $\langle 001 \rangle$, $\langle 110 \rangle$ and $\langle 010 \rangle$ directions, respectively,^[53–55]

$$A_1 = A_2 = \frac{2C_{55}}{C_{11} - C_{13}}, \quad (12)$$

$$A_3 = \frac{4C_{55}}{C_{11} + C_{33} - 2C_{13}}. \quad (13)$$

Values of A , A_1 , A_2 , and A_3 differ from 1, indicating the anisotropic character of the cubic and hexagonal structures. The Kleinman parameter ξ is an important parameter to describe the relative position of cation and anion sub-lattices and the material resistance to bond bending against bond stretching. Here the ξ parameter can be expressed as^[56]

$$\xi = \frac{C_{11} + 8C_{12}}{7C_{11} + 2C_{12}}. \quad (14)$$

The ξ value in the L1₂ structure is found to be very close to that in the D0₂₄ structure. To better define the hardness of our compound, Vickers hardness H_v is calculated using a theoretical model,^[57–59]

$$H_v = 0.92 \left(\frac{G}{B} \right)^{1.137} G^{0.708}. \quad (15)$$

The calculated hardness value for the cubic structure is 11.62 GPa (12.44 GPa) using the GGA (LDA) method. The values for the hexagonal structure are 6.99 GPa using the GGA and 6.86 GPa using the LDA, indicating that hardness of cubic Pt₃Zr is the highest. The calculated H_v values for L1₂ and D0₂₄ are under the superhardness limit (≥ 40 GPa). There are no experimental or theoretical results available about the mechanability index, anisotropy factor, Kleinman parameter and hardness for comparison.

Table 3. Calculated bulk modulus B (GPa), shear modulus G (GPa), Young's modulus E (GPa), Pugh's index B/G , B/C_{44} ratio, Poisson's ratio ν , anisotropic parameter A , Kleinman parameter ξ , and Vickers hardness H_v (GPa).

Structure		B	G	E	B/G	B/C_{44}	$C_{12} - C_{44}$	ν	A	ξ	H_v
L1 ₂	present GGA	240.43	116	300	2.072	1.72	42.10	0.29	0.59	0.632	11.62
	present LDA	271.29	129.62	335.43	2.092	1.73	49.52	0.29	0.60	0.636	12.44
	other ^[24,27,39]	232 ^a , 275 ^b	105 ^a , 113 ^a , 129 ^b	274 ^a , 335 ^b	2.50 ^a , 2.13 ^b , 2.05 ^a		77 ^a	0.29 ^a			
D0 ₂₄	present GGA	232.04	86.13	229.35	2.69	3.29	107.65	0.33	$A_1 = 0.70, A_3 = 0.63$	0.623	6.99
	present LDA	258.14	98.04	261.07	2.63	3.35	142.36	0.33	$A_1 = 0.58$	0.647	7.86
	other ^[39]	280 ^a	106 ^a		2.64 ^a			0.31 ^a	$A_2 = 0.73$		

^aData from the PBE-GGA method. ^bData from the LDA method.

3.3. Debye temperature

The Debye temperature θ_D is a characteristic parameter of numerous thermal solid properties such as specific heat, thermal conductivity, melting temperature and lattice vibration. Moreover, θ_D reflects the binding force between atoms. The higher the θ_D , the stronger the covalent bonding. Here θ_D can be calculated from the average acoustic velocity as follows:^[60]

$$\theta_D = \frac{h}{k} \left[\frac{3n}{4\pi} \left(\frac{N_A \rho}{M} \right) \right]^{1/3} v_m, \quad (16)$$

where h is Plank's constant, k Boltzmann's constant, N_A Avogadro's number, n the number of atoms per formula unit, ρ is the density, M the molecular mass per formula unit, and v_m the average acoustic velocity expressed as

$$v_m = \left[\frac{1}{3} \left(\frac{2}{v_s^3} + \frac{1}{v_l^3} \right) \right]^{1/3}, \quad (17)$$

where $v_s = \left(\frac{3B+4G}{3\rho} \right)^{1/2}$ and $v_l = (G/\rho)^{1/2}$ are the shear and longitudinal acoustic wave velocities, respectively.^[61,62]

Table 4. Calculated shear, longitudinal and average acoustic velocities (in m/s), i.e., v_s , v_l , and v_m , as well as Debye temperature θ_D (in K), melting temperature (in K).

Structure		v_s	v_l	v_m	θ_D	$T_m \mp 300$ K
L1 ₂	present GGA	2614.93	4826.08	2917.95	340.90	2665.16
	present LDA	2685.53	4972.83	2998.49	356.10	2926.02
	other ^[24,63]				342 ^b	2552 ^a
D0 ₂₄	present GGA	2257.23	4539.82	2532.69	295.52	
	present LDA	2342.46	4665.15	2627.15	312.25	
	other ^[24]					2427 ^a

^aData from the PBE-GGA method. ^bData from the LDA method.

The calculated v_m , v_l and v_s are displayed in Table 4. Acoustic velocities for the cubic structure are the highest, indicating that acoustical wave's propagation in the cubic structure is faster than that in the hexagonal structure. Debye temperature of cubic Pt₃Zr is the largest. Large values of θ_D indicate the strong covalent bond Pt–Zr of the cubic and hexagonal Pt₃Zr compound. The melting temperature is a significant parameter in engineering science. For the cubic structure, the calculated value of T_m is 2665 \mp 300 K (2926 \mp 300 K) using the GGA (LDA) method, which makes Pt₃Zr promising for high temperature applications.

3.4. Density of states

To better understand the structural stability and the bonding characteristics of the Pt₃Zr compound, total density of states (TDOS) and partial density of states (PDOS) are calculated using the GGA and LDA methods. Figure 3 gives the TDOS and PDOS of the Pt₃Zr compound in the D0₂₄ and L1₂ structures with the GGA approximation. The Fermi level is situated at 0 eV. The TDOS histogram of L1₂-Pt₃Zr (Fig. 3(a)) illustrates that the energy range from –10 eV to –0.67 eV at the bonding states is dominated by the Pt-5d states. However, in the above range the Fermi level from 0 to 9 eV at the

anti-bonding states is dominated by the hybridization of Pt-5d and Zr-4d states. This result agree very well with those obtained by Pan *et al.*^[24,26,27] The contribution of Zr-s, p and Pt-s, p in the PDOS of L1₂-Pt₃Zr is negligible. Furthermore, the main bonding peak is situated at –3.66 eV and the main anti-bonding peak, coming from a strong hybridization between Pt-d and Zr-d states, is situated in the energy range 0.42–1.1 eV.

It is known that for the hexagonal structure, Pt and Zr atoms occupy two positions (Pt1, Pt2, Zr1 and Zr2). Figure 3(b) illustrates the TDOS and PDOS histograms of D0₂₄-Pt₃Zr. It shows that the energy range from –9.25 eV to –0.21 eV is dominated by Pt1-5d and Pt2-5d states while the energy range from 0.70 eV to 9.28 eV is dominated by the hybridization of Pt1-d, Pt2-d, Zr1-d, and Zr2-d states. Moreover, the PDOS curves show that the orbital d of Zr1 and Zr2 atoms split into three levels: d_z^2 , $(d_{xy}, d_x^2 - d_y^2)$ and $(d_{xz} - d_{yz})$; while Pt1-d and Pt2-d orbitals into five levels: d_z^2 , $d_x^2 d_y^2$, d_{xy} , d_{xz} , and d_{yz} .

Figures 3 illustrates the existence of a deep-valley-shaped pseudo gap separating the bonding and anti-bonding states. The pseudo gap is formed from the large hybridization between Zr-4d states and Pt-5d states. The existence of the pseudo gap reflects a strong metallic character of the Pt₃Zr compound. Otherwise, The Fermi level is on the anti-bonding side for the cubic structure and exactly on the pseudo gap for the hexagonal system, indicating that D0₂₄-Pt₃Zr is predicted to be more stable than the L1₂-Pt₃Zr compound. This result is similar to that obtained by Popoola *et al.*^[39,63] Furthermore, the total density of states at Fermi level, $N(E_F)$, reflects the material electronic conductivity. The values of $N(E_F)$ of cubic and hexagonal Pt₃Zr are listed in Table 5. It is shown that $N(E_F)$ of D0₂₄-Pt₃Zr (0.52 states/eV) is lower than that of L1₂-Pt₃Zr (0.55 states/eV), indicating that the Pt₃Zr hexagonal structure is slightly more stable than the cubic structure. Moreover, we can deduce that electrical conductivity in the cubic structure is better than that in the hexagonal structure.

Furthermore, $N(E_F)$ is correlated to the electronic specific heat as follows:

$$\gamma = \frac{1}{3} \pi^2 k_B^2 N(E_F), \quad (18)$$

where k_B is the Boltzmann constant. At low temperature, the electronic specific heat has a large contribution in the material heat capacity. Table 5 regroups the calculated values of γ for cubic and hexagonal system. It is clear that γ of L1₂-Pt₃Zr is higher than that of D0₂₄-Pt₃Zr, indicating that the heat capacity of cubic structure is the highest. The values of DOS (N_{\min}) in the minimum of pseudogap of L1₂-Pt₃Zr (0.01 states/eV) is smaller than that of D0₂₄-Pt₃Zr (0.47 states/eV), where this minimum is situated at $E(N_{\min}) = -0.34$ eV and -0.08 eV for the cubic and hexagonal structures, respectively. The calculated values of N_{\min} and $E(N_{\min})$ are listed in Table 3.

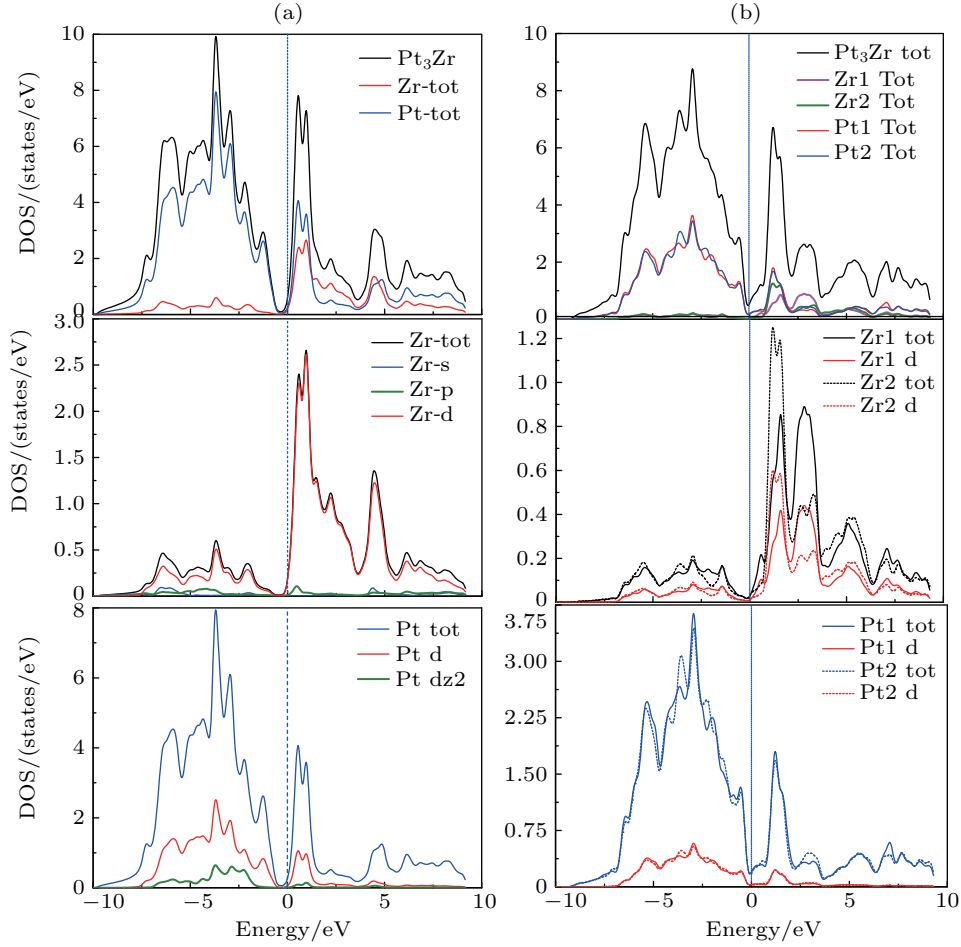


Fig. 3. Total and partial densities of states of Pt_3Zr : (a) L1_2 structure, (b) D0_{24} structure.

Table 5. Total and partial density of states at Fermi level ($N(E_F)$), minimum of DOS (N_{\min}), energies at N_{\min} ($E(N_{\min})$), number of bonding electrons (n_b) and electronic specific heat (γ) of cubic and hexagonal Pt_3Zr .

		$N(E_F)/(\text{states/eV})$	$N_{\min}/(\text{states/eV})$	$E(N_{\min})/\text{eV}$	Elect specific heat $\gamma/\text{mJ}\cdot\text{mol}^{-1}\cdot\text{K}^{-2}$	n_b
L1_2	Our GGA	Pt_3Zr : 0.55	Pt_3Zr : 0.1	-0.34	1,30	7.26
		Pt: 0.25	Pt: 0.06			
		Zr: 0.16	Zr: 0.02			
D0_{24}	Our GGA	Pt_3Zr : 0.52	Pt_3Zr : 0.47	-0.08	1.23	5.63
		Pt: 0.18	Pt: 0.16			
		Zr: 0.03	Zr: 0.02			

To further elucidate the bonding characteristics of the Pt_3Zr compound, the numbers of bonding electrons per atom for cubic and hexagonal Pt_3Zr , n_b , have been calculated. Table 5 illustrates that the n_b values for $\text{L1}_2\text{-Pt}_3\text{Zr}$ and $\text{D0}_{24}\text{-Pt}_3\text{Zr}$ are 7.26 and 5.63, respectively.

3.5. Optical properties

Optical properties of materials permit to understand their nature and describe their response to the electromagnetic radiations. These properties are strongly related to the electronic transition between occupied and unoccupied states. Study of materials optical nature provides good insight for their usage in optoelectronic devices. The complex dielectric function $\varepsilon(\omega)$ is known to determine the material response to the electromagnetic field and consists of two parts: $\varepsilon(\omega) =$

$\varepsilon_1(\omega) + i\varepsilon_2(\omega)$. The imaginary part $\varepsilon_2(\omega)$ describes the material's absorption behavior and related to the electronic band structure as follows:^[64–67]

$$\varepsilon_2(\omega) = \frac{4\pi^2 e^2}{m^2 \omega^2} \sum_{i,j} \int |\langle i|M|j \rangle|^2 f_i(1-f_j) \times \delta(E_f - E_i - \hbar\omega) d^3k, \quad (19)$$

where M is the dipole matrix, i and j are the initial and final states respectively, f_i is the Fermi distribution function for the i^{th} state, E_i is the energy of electron in the i^{th} state with wave vector k , and ω denotes the frequency of the incident wave. The real part $\varepsilon_1(\omega)$ of the dielectric function gives the information about the polarizability of the material and can be calculated from the imaginary part using the Kramers–Kronig

relation:^[67,68]

$$\varepsilon_1(\omega) = 1 + \frac{2}{\pi} P \int_0^{\infty} \frac{\omega' \varepsilon_2(\omega')}{\omega'^2 - \omega^2} d\omega', \quad (20)$$

where P stands for the principal value of the integral. There are two contributions to the dielectric function: interband transitions describing transitions between valence and conduction bands and intraband transitions describing transitions occurring inside the valence or conduction band.

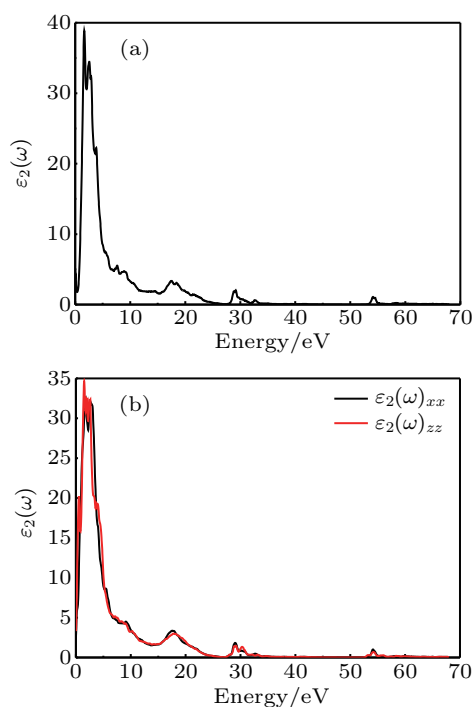


Fig. 4. Imaginary part of the dielectric function versus energy for the (a) cubic and (b) hexagonal Pt_3Zr intermetallic compound with the PBE-GGA method.

Optical properties of the Pt_3Zr intermetallic compound have been calculated using ab-initio calculations implemented in the wien2k code with the GGA exchange-correlation method for the cubic and hexagonal structures. To calculate the dielectric function, a dense k -mesh (365 k -points) in the irreducible Brillouin zone has been used. This study has been carried out for a large range of energy (0–70 eV). For the hexagonal structure, $\varepsilon(\omega)$ have two independent components: $\varepsilon_{xx}(\omega)$ corresponding to a parallel phonon polarization to c -axis and $\varepsilon_{zz}(\omega)$ corresponding to a perpendicular light polarization. Figures 4(a) and 4(b) illustrate the $\varepsilon_2(\omega)$ spectra of Pt_3Zr as a function of photon energy for the cubic and hexagonal structures, respectively. We show that the threshold energy is 0 eV for $\text{L1}_2\text{-Pt}_3\text{Zr}$ and $\text{D0}_{24}\text{-Pt}_3\text{Zr}$. For the cubic system, $\varepsilon_2(\omega)$ exhibits seven peaks located at 1.61 eV, 2.61 eV, 7.70 eV, 17.5 eV, 29.10 eV and 54.11 eV, which indicate the high phonon absorption in the energy values. Obviously, $\varepsilon_2(\omega)$ becomes zero in the energy ranges of 26.38–27.80 eV, 35.56–53.32 eV, and >62 eV, indicating that the cubic Pt_3Zr becomes transparent in these energy ranges. For the

hexagonal structure (Fig. 4(b)), $\varepsilon_2(\omega)_{xx}$ and $\varepsilon_2(\omega)_{zz}$ also exhibit seven peaks with a considerable anisotropy in the range 0–10 eV.

Moreover, the imaginary part reflects the electronic structure of the material. At low energies (0–10 eV), the imaginary part is characterized by considerable intraband transitions of free electrons, where the density of states of Pt-5d is dominant. However, the interband behavior is dominant in high energy area (< 25 eV) with a transition from Pt-5d states of valence band below the Fermi level to Zr-4d states of conduction band above the Fermi level.

The real part of the dielectric function $\varepsilon_1(\omega)$ is displayed in Fig. 5. For the cubic system (Fig. 5(a)), the static value $\varepsilon_1(\omega)$ at 0 eV is 35.79. From this value, $\varepsilon_1(\omega)$ starts increasing and reaches its maximum of 44.28 at 1.11 eV (1117 nm) in infrared (IR) region, then it decreases and becomes zero at 2.85 eV (435 nm). For the ranges 2.98–12.88 eV and 18.32–25.41 eV, $\varepsilon_1(\omega)$ takes negative values. The $\varepsilon_1(\omega)$ spectra of the hexagonal Pt_3Zr is illustrated in Fig. 5(b). We show that the static constant value is 44.27 and 50.6 for $\varepsilon_2(0)_{xx}$ and $\varepsilon_2(0)_{zz}$, respectively. The maximum values of $\varepsilon_1(\omega)_{xx}$ and $\varepsilon_2(\omega)_{zz}$ appear at 0.58 eV (2137 nm) and 0.11 eV (11271 nm), respectively. Moreover, $\varepsilon_1(\omega)_{xx}$ becomes negative in the energy ranges 3.04–13.48 eV and 17.70–25.45 eV. In the energy ranges 3.71–13.48 eV and 18.05–25.45 eV, $\varepsilon_2(\omega)_{zz}$ takes negative values. We observe a considerable anisotropic behavior in the region 0–10 eV.

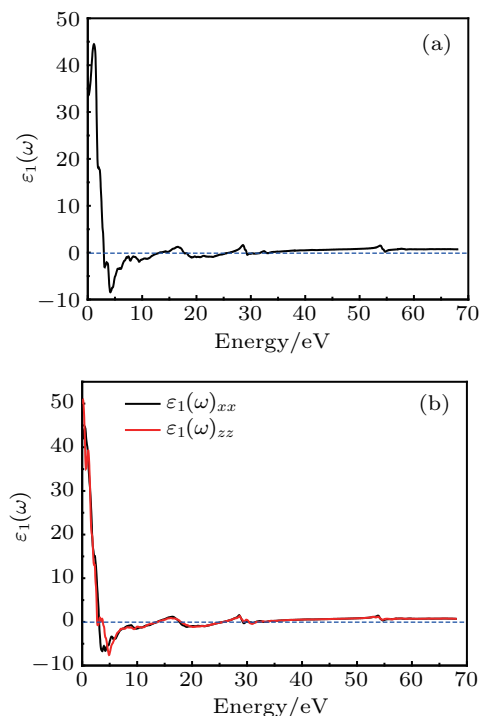


Fig. 5. Real part of dielectric function versus energy of the (a) cubic and (b) hexagonal Pt_3Zr intermetallic compound with the PBE-GGA method.

Other optical parameters such as absorption coefficient $\alpha(\omega)$, refractive index $n(\omega)$, energy loss function $L(\omega)$, reflectivity $R(\omega)$ and optical conductivity $\sigma(\omega)$ can be calcu-

lated by knowing $\epsilon_1(\omega)$ and $\epsilon_2(\omega)$ as follows:^[69,70]

$$\alpha(\omega) = \frac{2\pi\omega}{c} \sqrt{\frac{|\epsilon| - \epsilon_1(\omega)}{2}}, \quad (21)$$

$$n(\omega) = \left[\frac{\epsilon_1^2(\omega) + \epsilon_2^2(\omega) + \epsilon_1(\omega)}{2} \right]^{1/2}, \quad (22)$$

$$L(\omega) = \frac{\epsilon_2(\omega)}{[\epsilon_1^2(\omega) + \epsilon_2^2(\omega)]}, \quad (23)$$

$$R(\omega) = \frac{[n(\omega) - 1]^2 + k(\omega)^2}{[n(\omega) + 1]^2 + k(\omega)^2}, \quad (24)$$

$$\text{Re}[\sigma(\omega)] = \frac{\omega}{4\pi} \epsilon_2(\omega), \quad (25)$$

where $K(\omega)$ is the extinction coefficient given by

$$K(\omega) = \left[\frac{\epsilon_1^2(\omega) + \epsilon_2^2(\omega) - \epsilon_1(\omega)}{2} \right]^{1/2}. \quad (26)$$

The absorption coefficient is an important optical parameter related to light intensity variation when light passes through the material. Here $\alpha(\omega)$ is proportional to the imaginary part of the dielectric function. Peaks and valleys in the absorption spectra are corresponding to the possible transition between states from the valence band to the conduct band. Figure 6 illustrates the absorption curves of Pt₃Zr for the cubic and hexagonal structures. For the cubic system (Fig. 5(a)), the maximum absorption occurs in the ultraviolet (UV) region at 29.29 eV (42.32 nm) with a high absorption power of $308.1 \times 10^4 \text{ cm}^{-1}$. For the hexagonal phase (Fig. 5(b)), we show an anisotropic behavior in the energy ranges 2.6–22.60 eV, 28.74–49.90 eV and 53–70 eV. The maximum absorptions for $\alpha(\omega)_{xx}$ and $\alpha(\omega)_{zz}$ are 29.25 eV (42.38 nm) and 30.61 eV (40.50 nm), respectively, in the UV region.

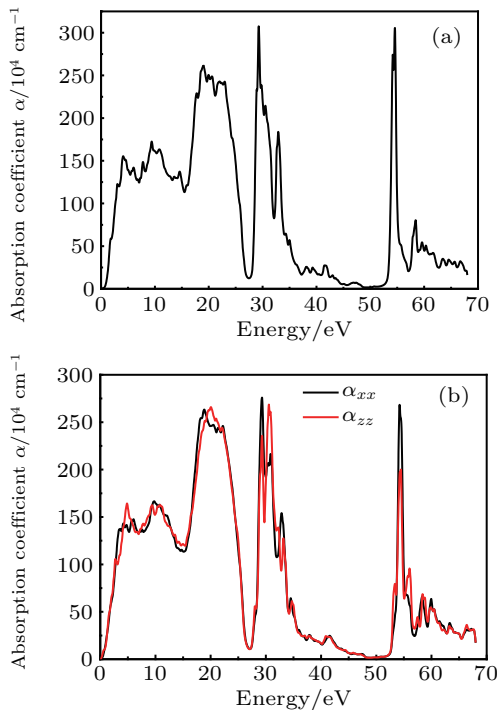


Fig. 6. Absorption coefficient of the (a) cubic and (b) hexagonal Pt₃Zr intermetallic compound as a function of photon energy with the PBE-GGA method.

The refractive index $n(\omega)$ (displayed in Fig. 7) is a significant physical parameter corresponding to the measurement of the phase velocity and the attenuation of electromagnetic wave in a medium. At $\omega = 0$, the static refractive index $n(0)$ can be determined by^[71] $n(0) = [\epsilon(0)]^{1/2}$. For L1₂-Pt₃Zr, the refractive index increases with lower energies (0.1–1.35 eV) and attains a maximum value of 6.86 at 1.35 eV (918.40 nm) in IR region, while it exhibits decreasing tendency for higher energy values. Here $n(\omega)$ takes the values less than unity for energy ranges: 10.69–13.40 eV, 18.84–28 eV, 30–52.40 eV and above 54.23 eV. Furthermore, the obtained value of $n(0)$ is 6.08.

For D0₂₄-Pt₃Zr, the maximum values of $n(\omega)_{xx}$ and $n(\omega)_{zz}$ are 7.15 and 6.73 given at 0.49 eV (2530.28 nm) and 0.10 eV (12398.42 nm) in IR region, respectively; $n(0)_{xx}$ and $n(0)_{zz}$ are 6.63 and 7.08, respectively. Moreover, the energy ranges corresponding to refractive index values less than 1 are 10.63–14.49 eV, ~18.70–~28 eV, 29.13–52.5 eV and above 54 eV.

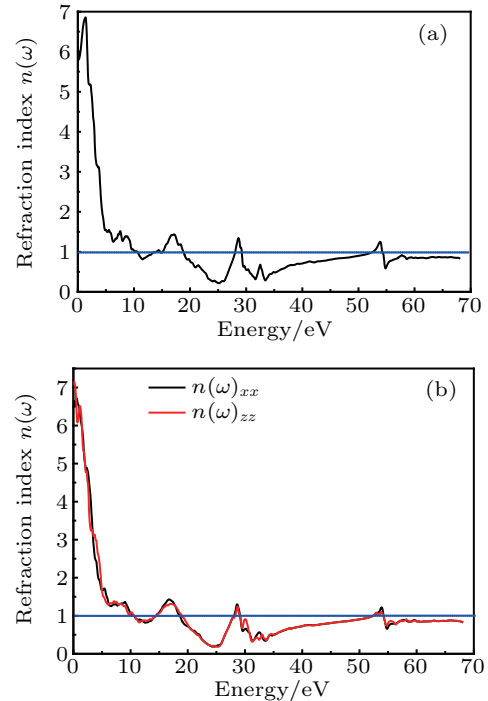


Fig. 7. Refractive index of the (a) cubic and (b) hexagonal Pt₃Zr intermetallic compound as a function of photon energy with the PBE-GGA method.

The electron energy loss function is shown in Fig. 8. This important optical parameter is proportional to the energy, in a unit of length, of a fast electron transverse in a material. The main peak in the loss function spectra is known as the plasmon peak, corresponding to the plasma resonance. The maximum values of $L(\omega)$ is given in UV region at 26.20 eV ($6.33 \times 10^4 \text{ Hz}$) for the cubic structure. However, the resonant energy loss for the hexagonal system is seen at 25.78 eV ($6.23 \times 10^{15} \text{ Hz}$) in UV region. The resonant energy indicates the transition energy from metallic to dielectric properties (starting energy of interband transitions).

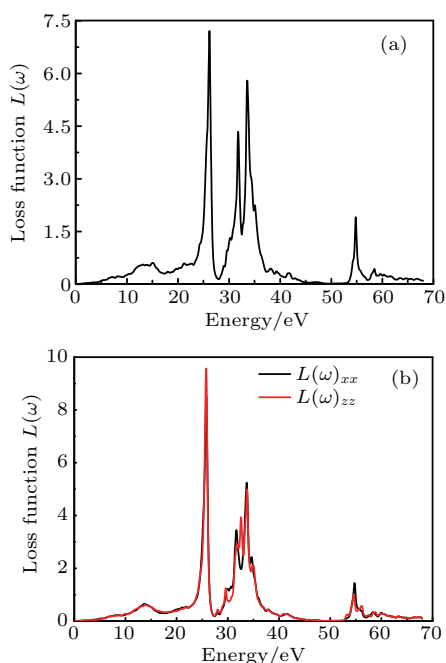


Fig. 8. Loss function of the (a) cubic and (b) hexagonal Pt_3Zr intermetallic compound as a function of photon energy with the PBE-GGA method.

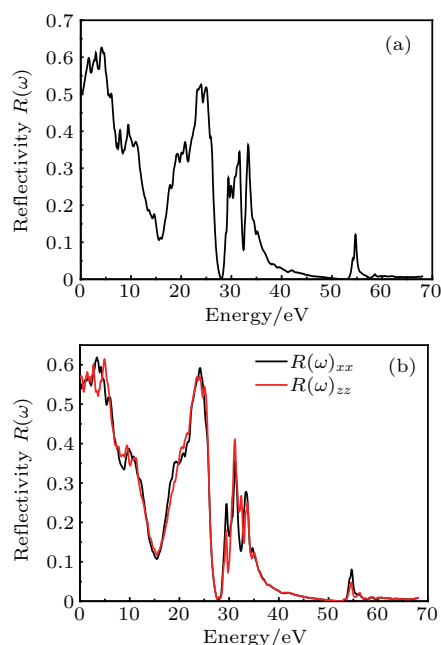


Fig. 9. Reflectivity of the (a) cubic and (b) hexagonal Pt_3Zr intermetallic compound as a function of photon energy with the PBE-GGA method.

The optical reflectivity $R(\omega)$ is the ratio between the reflected wave energy to the incident wave energy. $R(\omega)$ spectra of Pt_3Zr are displayed in Fig. 9. For the cubic structure, the maximum value of $R(\omega)$ is about 0.62, which occurs at 4.22 eV (293.80 nm) in UV region. Reflectivity becomes zero at 27.92 eV (44.40 nm) and in the region from 51 eV to 53 eV (24.31–23.39 nm), indicating that the material becomes transparent in these energies values. For the hexagonal structure, we observe an anisotropic structure. The main peak of $R(\omega)_{xx}$ is obtained at 3.41 eV (363.6 nm) with a reflectivity of 0.61. The same reflectivity value for $R(\omega)_{zz}$

tend to zero at 27.72 eV (44.72 nm). We can conclude that Pt_3Zr with a strong reflectivity (of 60%) in UV region can be considered as a promising material for coatings in this range.

Plots of the optical conductivity versus energy are shown in Fig. 10. It is shown that optical conductivity starts from zero, indicating that Pt_3Zr has no band gap. For the $L1_2$ system, the highest peak is obtained at 2.93 eV (423.15 nm) with a magnitude of $12608.09 \Omega^{-1}\cdot\text{cm}^{-1}$. For the D0_{24} structure, the maximum photoconductivity is $12883.24 \Omega^{-1}\cdot\text{cm}^{-1}$ and $11410.40 \Omega^{-1}\cdot\text{cm}^{-1}$ for $\sigma(\omega)_{xx}$ and $\sigma(\omega)_{zz}$, respectively, obtained at 3.04 eV (407.84 nm) and 2.65 eV (467.86 nm) energies.

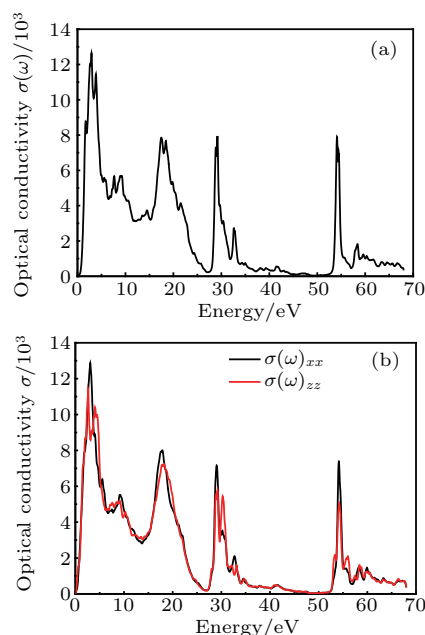


Fig. 10. Conductivity of the (a) cubic and (b) hexagonal Pt_3Zr intermetallic compound as a function of photon energy with the PBE-GGA method.

Furthermore, intraband transitions of free electrons at low photon energies correspond to the large values of the optical reflectivity, absorption coefficient and photoconductivity. When $\epsilon_2(\omega)$ attains a minimum, optical properties come from Pt-5d states with intraband transitions to interband transitions of Pt-5d states below the Fermi level to Zr-4d states at the Fermi level. This indicates the optical properties for transitions of metallic-to-dielectric behavior. Unfortunately, there are no experimental or theoretical data available in the literature for the optical properties of the Pt_3Zr compound for comparison.

4. Conclusion

In summary, we have investigated structural, elastic, electronic and optical properties of the Pt_3Zr intermetallic compound in cubic and hexagonal structures with the FP-LAPW method. The results predict that the hexagonal phase is more stable than the cubic phase. The calculated elastic constants illustrate the mechanical stability of our compound. Values

of Young's modulus indicate that cubic Pt₃Zr is much stiffer than hexagonal Pt₃Zr. Calculated bulk modulus, shear modulus and Vickers Hardness show that hexagonal Pt₃Zr has the highest hardness. Poisson's ratio reveals the metallic bonding behavior of cubic and hexagonal Pt₃Zr. Pugh's index and Cauchy pressure indicate the ductile nature of our material. Our compound exhibits an anisotropic character. Cubic Pt₃Zr has the largest Debye and melting temperature, indicating the strong covalent nature of this compound. Computed density of states shows that hexagonal Pt₃Zr electronically is more stable than cubic Pt₃Zr. Considering $N(E_F)$ and electronic specific heat values, we can deduce that electrical conductivity, melting temperature and heat capacity in the cubic structure are better than those in the hexagonal structure. Optical properties of the Pt₃Zr compound have been investigated using the real and imaginary parts of dielectric function. Maximum absorption and reflectivity are obtained in UV region for cubic and hexagonal Pt₃Zr. The refractive index of hexagonal Pt₃Zr (in IR region) is the highest. The electron energy loss function has also been computed. Optical conductivity $\sigma(\omega)$ spectrum illustrates that highest values of $\sigma(\omega)$ are obtained for the hexagonal structure according to the zz direction. Moreover, intra and inter-band transitions have been discussed. We can conclude that our study is valuable for the future applications of the Pt₃Zr intermetallic compound as a structural material.

References

- [1] Chen X Q, Fu C L and Morris J R 2010 *Intermetallics* **18** 998
- [2] Pan Y, Guan W M and Zhang K H 2013 *Physica B* **427** 17
- [3] Sheng L Y, Zhang W, Guo J T, Wang Z S, Ovcharenko V E, Zhou L Z and Ye H Q 2009 *Intermetallics* **17** 572
- [4] Liu C T, Stringer J, Mundy J N, Horton L L and Angelini P 1997 *Intermetallics* **5** 579
- [5] Fairbank G B, Humphreys C J, Kelly A and Jones C N 2000 *Intermetallics* **8** 1091
- [6] Miura S, Honma K, Terada Y, Sanchez J M and Mohri T 2000 *Intermetallics* **8** 785
- [7] Gao Y, Guo C, Li C and Du Z 2010 *Int. J. Mater. Res.* **101** 819
- [8] Yamabe Mitarai Y, Ro Y and Murakami H 1998 *Metall. Mater. Trans. A* **29** 537
- [9] Yamabe Mitarai Y, Ro Y, Maruko T and Murakami H 1998 *Scr. Mater.* **40** 109
- [10] Yamabe Mitarai Y, Ro Y, Maruko T and Murakami H 1999 *Intermetallics* **7** 49
- [11] Yamabe Mitarai Y, Nakazawa S and Harada H 2000 *Scr. Mater.* **43** 1059
- [12] Yamabe Mitarai Y and Aoki H J 2003 *Alloys Compd.* **359** 143
- [13] Luo J, Li M, Li H and Yu W 2009 *Mater. Sci. Eng. A* **505** 88
- [14] Odusote J K, Cornish L A and Chown L H 2012 *Corros. Sci.* **63** 119
- [15] Alam M Z, Kamat S V, Jayaram V and Das D K 2013 *Acta Mater.* **61** 1093
- [16] Liebscher C H and Glatzel U 2014 *Intermetallics* **48** 71
- [17] Hill P J, Mitarai Y Y and Wolff I M 2001 *Scr. Mater.* **44** 43
- [18] Jiang C, Sordelet D J and Gleeson B 2005 *Phys. Rev. B* **72** 184203
- [19] Yamabe Y, Koizumi Y, Murakami H, Maruko Y R T and Harada H 1996 *Scr. Mater.* **35** 211
- [20] Srikrishnan V and Ficalora P 1974 *Metall. Mater. Trans.* **5** 1471
- [21] Brewer L 1967 *Acta Metall.* **15** 553
- [22] Hum-Rothery W 1968 *Prog. Mater. Sci.* **13** 229
- [23] Pan Y, Guan W, Wen M, Zhang J, Wang C and Tan Z 2014 *J. Alloys Compd.* **585** 549
- [24] Yong P, Lin Y, Wang X, Chen S, Wang L, Tong C and Cao Z 2015 *J. Alloys Compd.* **643** 49
- [25] Bai X, Li J H, Dai Y and Liu B X 2013 *Trans. Nonferrous Met. Soc. Chin.* **23** 3704
- [26] Pan Y, Wang S, Jia L and Zhang X 2017 *RSC Adv.* **7** 54772
- [27] Pan Y, Lin Y H, Wang H, Guo J M, Singh A and Fu C Y 2016 *Comput. Mater. Sci.* **111** 74
- [28] Li H, Choi J J, Schmolzer W M, Weilach C, Rameshan C, Mittendorfer F et al 2015 *J. Phys. Chem. C* **119** 2462
- [29] Antlanger M, Schmolzer W M, Pavelec J, Mittendorfer F, Redinger J, Varga P et al Diebold U 2012 *Phys. Rev. B* **86** 035451
- [30] Lu Y, Lu W G and Wang L 2017 *Chin. Phys. Lett.* **34** 017102
- [31] Li X Y, Huang C, Zhu Y, Li J B, Fan J Y, Pan Y F, Shi D N and Ma C L 2018 *Acta Phys. Sin.* **67** 137101 (in Chinese)
- [32] Blaha P, Schwarz K G Madsen K H, Kvasnicka D and Luitz J 2001 (Universitat Wien Austria: WIEN2K, Karlheinz Schwarz Techn.)
- [33] Hohenberg P and Kohn W 1964 *Phys. Rev.* **136** 86
- [34] Perdew J P, Burke S and Ernzerhof M 1996 *Phys. Rev. Lett.* **77** 3865
- [35] Perdew J P and Zunger A 1924 *Phys. Rev. B* **23** 048
- [36] Stalick J K and Waterstrat R M 2007 *J. Alloys Compd.* **430** 123
- [37] Stampel C, Mannstadt W, Asahi R and Freeman A J 2001 *Phys. Rev. B* **63** 155106
- [38] Johannesson G H, Bligaard T, Ruban A V, Skriver H L, Jacobsen K W and Norskov J K 2002 *Phys. Rev. Lett.* **88** 255506
- [39] Popoola A I, Chown L H and Cornish L A 2014 *Turkish J. Phys.* **38** 10
- [40] Born M and Huang K 1998 *Dynamical Theory of Crystal Lattices* (New York: Oxford University Press)
- [41] Born M and Huang K 1956 *Dynamical Theory of Crystal Lattices* (New York: Oxford University Press)
- [42] Jamal M 2012 *Hex-elastic*
- [43] Hill R 1952 *Proc. Phys. Soc. London. A* **65** 349
- [44] Voigt W 1928 *Lehrbuch der Kristallphysik* (Teubner: Leipzig)
- [45] Reuss A and Angew Z 1929 *Math. Mech.* **9** 49
- [46] Mayer B, Anton H, Bott E, Methfessel M, Sticht J and Schmidt P C 2003 *Intermetallics* **11** 23
- [47] Chen Y M, Cheng W, Liao B and Zhang X 2013 *Int. J. Mod. Phys. B* **27** 1350095
- [48] Sun Z, Music D, Ahuja R and Schneider J M 2005 *Phys. Rev. B* **71** 193402
- [49] Vitos L, Korzhavyi P A and Johansson B 2003 *Nat. Mater.* **2** 25
- [50] Lincoln R C, Koliwad K M and Ghate P B 1967 *Phys. Rev.* **157** 463
- [51] Puttlitz K J, Stalter K A 2004 *Handbook of Lead-Free Solder Technology for Microelectronic Assemblies* (New York: Marcel Dekker)
- [52] Sundareswari M, Ramasubramanian S and Rajagopalan M 2010 *State Commun.* **150** 2057
- [53] Mio N, Zhou B J and Sun Z 2011 *Comput. Mater. Sci.* **50** 1559
- [54] Ren B, Lu D, Zhou R, Ji D, Hu M and Feng J 2018 *Chin. Phys. B* **27** 107102
- [55] Longke B, Deyi Q, Zhuangzhuang K and Yonghua D 2019 *Solid State Sci.* **98** 106027
- [56] Harrison A A 1989 *Electronic Structure and Properties of Solids* (New York: Dover)
- [57] Deyi Q, Longke B, Zhuangzhuang K and Yonghua D 2019 *Mater. Res. Express* **6** 116569
- [58] Tian Y, Xu B, Zhao Z 2012 *Int. J. Refract. Met. Hard Mater* **33** 93
- [59] Zhuangzhuang K, Mingjun P, Yong S, Deyi Q and Longke B 2019 *Phys. B: Condens. Matter* **571** 222
- [60] Anderson O L 1963 *J. Phys. Chem. Solids.* **24** 909
- [61] Huang Z, Zhao Y, Hou H and Han P 2012 *J. Phys. B* **407** 1075
- [62] Wachter P, Filzmoser M, Rebizant 2001 *Phys. B.* **293** 199
- [63] Popoola A I 2013 *PhD Dissertation* (Johannesburg: University of Witwatersrand)
- [64] Wooten F 1972 *Optical Properties of Solids* (New York: Academic Press)
- [65] Yang Z J, Guo Y D, Li J, Liu J C, Dai W, Cheng X L and Yang X D 2010 *Chin. Phys. B* **19** 077102
- [66] Yao G, Chen Y, An X Y, Jiang Z Q, Cao L H, Wu W D and Zhao Y 2013 *Chin. Phys. Lett.* **30** 067101
- [67] Saad Ta, Mubarak A A, Saher S, Jamil M I and Gilani S M 2019 *Chin. Phys. B* **28** 066101
- [68] Ahuja R, Eriksson O, Johansson B, Auluck S and Wills J M 1996 *Phys. Rev. B.* **54** 10419
- [69] Sun J, Wang H T, He J L and Tian Y J 2005 *Phys. Rev. B.* **71** 125132
- [70] Okoye C M I 2003 *J. Phys.: Condens. Matter.* **15** 5945
- [71] Fox M 2001 *Optical Properties of Solids* (New York: Oxford University Press)